Laser and Particle Beams (2001), *19*, 609–622. Printed in the USA.

DOI: 10.1017.S0263034601194085

Transport of electron beams and stability of optical windows in high-power e-beam-pumped krypton fluoride lasers

V.D. ZVORYKIN,[1] S.V. ARLANTSEV,[2] V.G. BAKAEV,[1] O.V. RANTSEV,[1] P.B. SERGEEV,[1] G.V. SYCHUGOV,[1] AND A.Yu. TSERKOVNIKOV[1]

[1]P.N. Lebedev Physical Institute, Russian Academy of Sciences, Leninsky Prospect 53, 119991 Moscow, Russia
[2]OKB "Granat," Volokolamskoe Shosse 95, 123424 Moscow, Russia

(RECEIVED 23 October 2000; ACCEPTED 24 May 2001)

Abstract

Two of the key issues of a krypton fluoride (KrF) laser driver for inertial fusion energy are the development of long life, high transparency pressure foils (to isolate vacuum in the electron beam diode from a working gas in the laser chamber), and the development of durable, stable, optical windows. Both of these problems have been studied on the single-pulse e-beam-pumped KrF laser installation GARPUN. We have measured the transport of electron beams (300 keV, 50 kA, 100 ns, 10×100 cm) through aluminum-beryllium and titanium foils and compared them with Monte Carlo numerical calculations. It was shown that 50-μm thickness Al-Be and 20-μm Ti foils had equal transmittance. However, in contrast to Ti foil, whose surface was strongly etched by fluorine, no surface modification nor fatal damages were observed for Al-Be foils after ~1000 laser shots and protracted fluorine exposure. We also measured the 8% reduction in the transmission of CaF_2 windows under irradiation by scattered electrons when they were set at 8.5 cm apart from the e-beam-pumped region. However an applied magnetic field of ~0.1 T significantly reduced electron scattering both across and along the laser cell at typical pumping conditions with 1.5 atm pressure working gas. Thus the e-beam-induced absorption of laser radiation in optical windows might be fully eliminated in an e-beam-pumping scheme with magnetic field guiding.

Keywords: Aluminum-beryllium foil transmittance and stability; E-beam-induced absorption in optical windows; E-beam-pumped high-power KrF laser

1. INTRODUCTION

Electron-beam-pumped krypton fluoride (KrF) lasers might be the best approach for inertial fusion energy (IFE). Numerous investigations, which have been carried out in the fields of both laser physics and laser–plasma interaction through the past two decades, were performed with single-pulse lasers of 100–10,000 J output energy: RAPIER (Swingle *et al.*, 1981), AURORA (Rosocha *et al.*, 1986, 1987; Turner *et al.*, 1990; Harris *et al.*, 1993), NIKE (Obenschain *et al.*, 1996; Pawley *et al.*, 1997), SPRITE and TITANIA (Shaw *et al.*, 1982, 1991, 1993; Divall *et al.*, 1996), ASHURA (Owadano *et al.*, 1989, 1993, 1996), GARPUN (Basov *et al.*, 1991, 1993; Zvorykin & Lebo, 1999). These have shown the main advantages of KrF lasers: high intrinsic (~12%) and wall-plug efficiencies (~2%) were achieved for this type of laser. Short fundamental wavelength ($\lambda = 248$ nm) and a broad bandwidth ($\Delta\nu \approx 3$ THz) are favorable for a high absorption of laser radiation in plasma, as well as for suppression of plasma instabilities and small target preheat by fast electrons. A design study for a 1 GWe IFE power plant, called SOMBRERO, has been carried out (Sviatoslavsky *et al.*, 1992; Von Rosenberg, 1992). The total laser energy was defined to be 3.4 MJ. This system should operate at 5 Hz, and have an overall system efficiency of 6.5%. To be economically warranted, laser drivers should cost no more than $180 per Joule, and have a durability between major maintenances $2 * 10^8$ shots. To obtain the desired laser energies in single pulses, it should be possible to extend the existing KrF laser technologies. In fact, there are several conceptual designs for large electron-beam-pumped KrF modules with output energies of 50–500 kJ (Lowenthal *et al.*, 1981; Hunter *et al.*, 1986; Sullivan & Von Rosenberg,

Address correspondence and reprint requests to: Dr. Vladimir D. Zvorykin, Russian Academy of Sciences, P.N. Lebedev Physical Institute, Leninsky pr.53, 119991 Moscow, Russia. E-mail: zvorykin@sci.lebedev.ru

1986; Sullivan, 1987; Ueda & Takuma, 1988; Sasaki *et al.*, 1989; Sullivan *et al.*, 1993, McGeoch *et al.*, 1997). In addition, it should be noted that successive integration of e-beam pumping with gas flow and acoustic technology and an optical extraction technique has been demonstrated earlier at EMRLD XeF laser, which produced multi-kW average power at 100 Hz repetition rate (rep-rate) during short 1-s bursts (Smiley, 1990).

A newly developed e-beam-pumped repetition-rate KrF laser system ELECTRA is being built at the Naval Research Laboratory (NRL). ELECTRA will establish the key technologies that will produce an efficient and reliable KrF laser. It will operate at 5 Hz with output energy up to 700 J and average power of a few kilowatts (Sethian *et al.*, 1998, 1999). The key problems to be solved are as follows: (1) durable and efficient high-voltage pulsed power supply for e-beam accelerators; (2) large-area cathodes to emit uniform 110 kA, 500 kV, 100 ns e-beams; (3) long lifetime and transparent pressure foil support structure for the injection of e-beams from accelerators into a laser cavity; (4) circulation loop to make working gas cool and quiet between subsequent shots; (5) reliable repetition-rate preamplifier; and (6) long lifetime large-size optical windows. The new technologies that are developed for the 700 J ELECTRA laser will be scalable to higher laser energies level of 30–100 kJ, which is necessary for the laser beam line of an IFE laser driver.

In this paper, we discuss two issues for rep-rate lasers: transport of high-current relativistic e-beams through different foil materials and the influence of scattered electrons on the transparency and durability of optical windows. In KrF lasers, e-beams of a large area are passed through foil windows from vacuum diodes into a laser cell. This foil window, with its associated foil-support structure (usually called a "hibachi") should have a transmittance of about 90%, be able to withstand the steady pressure difference between the diode and laser gas, and be able to survive the sudden, repetitive pressure impulse caused by the e-beam depositing its energy into the gas. In addition, the hibachi must be able conduct heat due to absorbed electrons, and be resistant to chemical attack from the fluorine, and hydrofluoric acid (HF). Titanium foils or Kapton (polyimide) films have been typically used in single-pulse large KrF laser installations (Sethian *et al.*, 1997a, 1997b). But these have a limited lifetime, which have been measured from several tens or hundreds of shots to 1000–10,000 shots (Divall *et al.*, 1995) in dependence on the design and operation conditions. Although the failure mechanism for the Ti foils is unknown, it may be due to low heat conductivity and a tendency for allotropic transformation at elevated temperatures. An iron alloy HOVAR foil was chosen for tests at a rep-rate KrF laser facility (Takahashi *et al.*, 1999), but a foil composed of an aluminum-beryllium (Al-Be) alloy might be the best choice due to its high strength (compared with Ti), excellent heat conductivity, and very low density (Webster & London, 1979). The latter is important because it determines the absorption of e-beam. Some benefits of Al-Be foil windows have been discussed earlier (Grigorev & Stepanov, 1990). This paper presents the first comprehensive investigation of Al-Be foil carried out with an e-beam-pumped large-aperture amplifier and preamplifier modules of the GARPUN KrF laser installation (Basov *et al.*, 1991, 1993). Direct comparison of the transparency of 50-μm thickness Al-Be foil manufactured by Russian industry and a convenient 20-μm Ti foil has been done using the Faraday cup technique. Durability of both foils was determined in a prolonged run of single-pulse experiments lasting up to 1000 shots. Statistics and morphology of typical damages of the foil and its resistance to fluorine etching were investigated. In addition, a Monte Carlo numerical code has been developed to calculate e-beam transport through different foil materials, with the results compared with the experiments.

The other issue we investigated was the effect of beam electrons on the UV transmission of the windows in a KrF amplifier cell. In addition to intense UV laser light, the windows are exposed to etching by fluorine, and irradiation by bremsstrahlung X rays and scattered energetic electrons. Fast electrons could induce additional transient and residual absorption of laser radiation (Barabanov *et al.*, 1992; Amosov *et al.*, 1993; Barabanov & Sergeev, 1995; Eliseev *et al.*, 1996), which, of course, would decrease the efficiency and durability of a KrF laser. Besides fused silica, which is commonly used in KrF lasers (although it has been known to degrade in the fluorine), calcium fluoride (CaF_2) is the most promising material for optical windows. CaF_2 is resistant to fluorine; it is relatively cheap and might be manufactured at a large size. But the data concerning CaF_2-induced absorption of UV laser radiation are rather inconsistent. In experiments with UV illumination at 200–300 Hz rep-rate by an industrial-grade discharge KrF laser (no e-beam and no X rays) it was demonstrated that there was no degradation in CaF_2 windows after $7.5 * 10^7$ pulses at 0.32 J/cm^2 fluence. This was in direct contrast to fused silica windows, in which transmission decreased by 4% after the same exposure (Krajnovich *et al.*, 1992). On the other hand, after several months of operation as windows of a single-pulse e-beam-pumped KrF amplifier, CaF_2 windows reduced their transmission significantly (Divall & Hirst, 1993). The residual absorption was believed to arise due to color centers formation, induced by the UV, X-ray and/or scattered e-beam irradiation.

The distributions of energy fluence of e-beams and scattered electrons have been measured at various pumping conditions in the middle of the laser chamber and away from the injected e-beams region at different distances along laser cell axis. We correlate this distribution with induced absorption measurements in CaF_2 samples. The influence of applied magnetic field of $\sim$0.1 T on e-beam scattering was investigated. The Monte Carlo numerical code was used to calculate the distribution of scattered electrons inside the laser cell. These were verified in the present experiments with the GARPUN laser of $16 \times 18 \times$

https://doi.org/10.1017/S0263034601194085 Published online by Cambridge University Press

100 cm active volume, then the code was applied to calculate the e-beam scattering and electron escape onto optical windows in the NRL repetition-rate $30 \times 30 \times 100$ cm ELECTRA laser. Transient and residual e-beam-induced absorption in CaF_2 windows has been determined in typical pumping conditions for large-scale KrF lasers.

2. LASER FACILITIES AND EXPERIMENTAL PROCEDURE

The experiments with two laser modules of the GARPUN installation have been performed to investigate e-beam transportation throughout Al-Be foil and to determine its stability in comparison with Ti foil. The Al-Be foil was manufactured by means of multistage hot rolling and annealing of the heterogeneous alloy. The alloy consisted of 50% weight amount of aluminum and 50% of beryllium, and had an average density of 2.2 g/cm^3. To make the foil safe to handle, both its sides were overcoated with a 2-μm aluminum layer, which was placed on the alloy surface before the rolling. The total thickness of the Al-Be foil was 50 μm.

The preamplifier laser module BERDYCH of $10 \times 10 \times 100$ cm active volume was adjusted for transmittance measurements of different foils. It was pumped with a single-side e-beam of 900 J total energy and ~100 ns pulse duration. The high-voltage power supply of the electron accelerator consists of a 7-stage Marx generator with 3.0 kJ energy storage at 400 kV pulsed voltage and a water-filled Blumlein forming line of 7.6 Ω wave impedance, which produced pulses of ~350 kV voltage. The layout of laser chamber (1) and vacuum diode (2) equipped for e-beam transport experiments is shown schematically in Figure 1. The cathode (3) of 100-cm length and 8-cm width had a convex-shaped emitting surface formed by a graphite fabric to prevent a "halo" effect and to insure uniform electron emission (Rosocha & Riep, 1987; Bakaev *et al.*, 1994). It was placed at 3-cm distance from the anode grid (4). The foil (5) was set 3 cm behind the grid and was supported by the hibachi structure (6). The hibachi ribs are 3 mm wide and 6 mm thick. The open areas between the ribs are 27 mm wide and 100 mm high. This would correspond to a geometric transparence of 90%, if one supposes that electrons have no velocity component transverse to the accelerating electric field. To prevent the e-beam from pinching due to its self-magnetic field, and to diminish the losses of electrons in a vacuum diode and scattered in a foil, an external pulsed magnetic field was applied collinearly to the electric field. It was produced by a solenoid (7) and reached maximum value of 0.065 T at 40 ms. The magnetic field was altered in experiments by varying the voltage at the capacitor bank of the solenoid's power supply. The e-beam current transmitted through the foil and foil support structure has been measured by means of a Faraday cup (8) set 1.7 cm behind the foil inside the laser chamber. The Faraday cup was evacuated down to 10^{-2} Torr. The graphite receiving plate of the Faraday cup with dimensions of 9.3×23 cm was slightly less than the height of the chamber. The stop (9) with variable gap was used to measure the electron beam distribution in the vertical (perpendicular to the cathode axis) direction. The Faraday cup was placed in different positions along the cathode to verify that the electron beam current was uniform. Additional Ti foils (10) were added in front of the Faraday cup to the measure attenuated e-beam current and to determine the energy distribution of electrons. A Rogowski coil (11), which enveloped a high-voltage bushing (12) with a conductor to the cathode, measured the total current in the vacuum diode during all measurements.

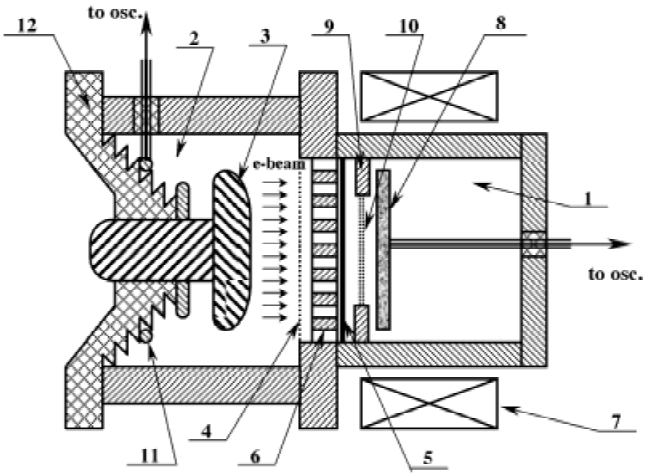

Fig. 1. Cross section of BERYCH laser module arranged for e-beam transport measurements. 1: Laser chamber; 2: vacuum diode; 3: cathode; 4: anode grid; 5: foil; 6: hibachi; 7: solenoid; 8: Faraday cup; 9: stops; 10: additional foil; 11: Rogowski coil; 12: bushing.

The main GARPUN module was arranged to measure the distribution of scattered electrons in conditions typical for a large-aperture e-beam-pumped KrF laser and to investigate transient and residual e-beam-induced absorption in CaF_2 samples. The stability of the Al-Be foil was determined simultaneously. The layout of these experiments is shown schematically in Figure 2a,b. The GARPUN module has a laser chamber (1) with dimensions of $19 \times 22 \times 140$ cm and output aperture of 16×18 cm. Two counterpropagating e-beams of an area 12×100 cm and with current density 50 A/cm^2 were generated in vacuum diodes (2) and coupled into the chamber from opposite sides. The pressure foils (3) were either 20-μm thickness Ti or 50-μm thickness Al-Be. They were supported by the hibachi structure (4) having ribs of 2 mm width, 10 mm thickness, and 8 mm interrib gaps. The e-beams were stabilized usually by a pulsed magnetic field of inductance $B \sim 0.1$ T, generated by a pair of solenoids (6) in a direction along the beams. The experiments have also been performed without magnetic field in order to understand its influence on e-beam scattering. The pulses of 350 kV accelerating voltage and 120 ns duration were delivered to a pair of cathodes (7) in each vacuum diode by four water-filled Blumlein forming lines with 7.6 Ω wave

https://doi.org/10.1017/S0263034601194085 Published online by Cambridge University Press

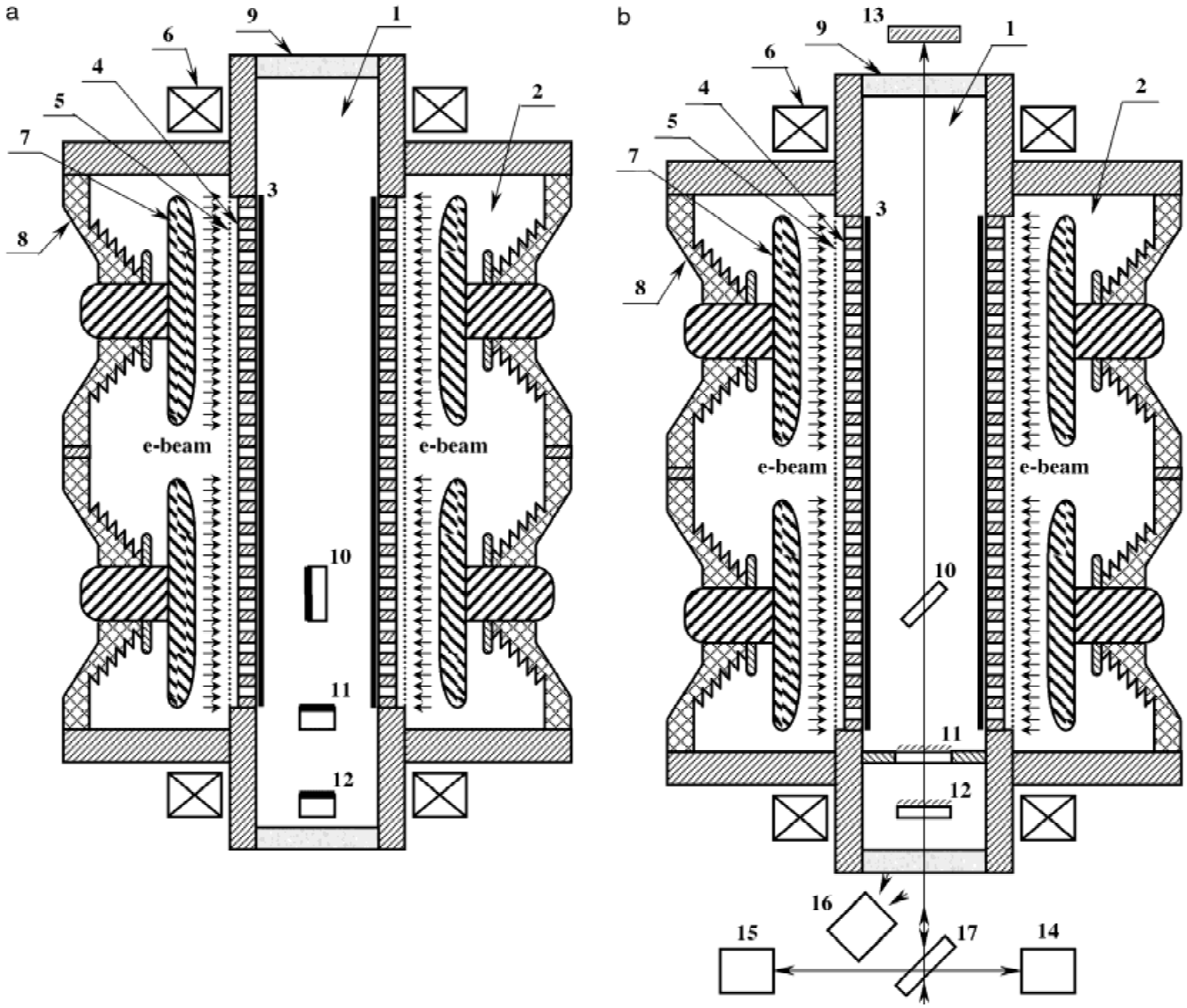

Fig. 2. (a) Cross section of GARPUN laser module arranged for e-beam scattering measurements. 1: Laser chamber; 2: vacuum diode; 3: foil, 4: hibachi; 5: anode grid; 6: solenoid; 7: cathode; 8: bushing; 9: output window; 10, 11, 12: calorimeters. (b) Cross section of GARPUN laser module arranged for e-beam-induced absorption measurements. 1: Laser chamber; 2: vacuum diode; 3: foil; 4: hibachi; 5: anode grid; 6: solenoid; 7: cathode; 8: brushing; 9: output window; 10, 11, 12: tested CaF_2 samples; 13: mirror; 14, 15, 16: photodiodes; 17: beam-splitter.

impedance. The lines were charged by a 7-stage, 14-kJ Marx generator.

3. MONTE CARLO NUMERICAL MODELING

The most accurate and universal description of the processes of electron transport in a medium is provided by the Monte Carlo method, which has been used earlier in calculations of the e-beam pumping of the GARPUN laser (Arlantsev *et al*., 1994). Its main advantage is that the real geometry and the structural features of the apparatus can be modeled. We used the "single-particle" approximation, ignoring the interaction of the beam electrons with one another. This neglect of the collective effects was justified by the fact that the external magnetic field was 1.5 times as high as the intrinsic magnetic field. The second requirement, suppression of the plasma instabilities, was also satisfied, since at typical gas densities, the frequency of collisions of the plasma electrons with neutral particles was higher than the instability growth rate. Under these conditions the main interactions between the e-beam and the medium were pair collisions of electrons with foil and gas atoms. These resulted in the excitation or ionization of atoms and elastic scattering of electrons. Radiative energy losses in elastic collisions could be ignored at the electron energies under consideration.

https://doi.org/10.1017/S0263034601194085 Published online by Cambridge University Press

The algorithm used to solve the problem included a calculation of the paths of individual electrons in the beam in the intervals between successive collisions, and modeling of the energy loss and scattering processes in collisions between electrons and atoms. We also studied the deceleration of high-energy secondary electrons, which were created by the ionization of atoms and were capable in turn of generating an avalanche of secondary electrons. The modeling began with selection of the initial energy of an electron, its coordinates, and direction of injection into the investigated region. Then the coordinates of the point of interaction of an electron with an atom were found by solving the equations of motion:

$$\frac{d\vec{P}}{dt} = e[v \times \vec{B}], \qquad \vec{P} = \frac{m_e \vec{v}}{\sqrt{1 - v^2/c^2}}, \qquad \frac{d\vec{S}}{dt} = \vec{v}, \tag{1}$$

where the path S traveled by an electron was calculated by solving the equation:

$$\int_0^s ds' Q(s') \exp\left[- \int_0^{s'} Q(s'')\, ds'' \right] = \xi. \tag{2}$$

Here, $Q = N\sigma_t$ is a product of the density of the scattering particles and the total collision cross section; ξ is a random number distributed uniformly in the interval (0, 1). For a homogeneous medium, Q is a constant and Eq. (2) can be transformed to the simple expression

$$S = -Q^{-1} \ln(1 - \xi). \tag{3}$$

The equations of motion (1) were solved numerically. When the point of collision was inside the selected region, the type of the collision was picked at random and then the energy loss and the scattering angle were found. The new collision point was then determined and the process repeated until the particle either left the investigated region or its energy became so low that it could be regarded as having come to rest. The angle and energy of the electrons escaping outside the selected region, as well as their total number, were determined.

Inelastic collisions of the beam electrons with atoms were considered on the assumption that the interaction could be treated in the same way as that of free electrons. In the relativistic case, the differential inelastic scattering cross section was described by the Moliere expression (Zerby & Keller, 1967):

$$\frac{d\sigma_n}{d\varepsilon} = 2\pi r_e^2 \frac{Z}{\beta^2 T} \left[\frac{1}{\varepsilon^2} - \frac{1}{\varepsilon(1-\varepsilon)} \frac{2T+1}{(T+1)^2} + \frac{1}{(1-\varepsilon)^2} + \frac{T^2}{(T+1)^2} \right], \tag{4}$$

where ε is the fraction of the energy lost by a primary electron in a collision; r_e is the classical radius of an electron; $\beta = v/c$; T is the electron energy in units of $m_e c^2$; Z is the nuclear charge of an atom.

Elastic collisions of electrons with atoms were considered as the scattering of electrons in the field of a nucleus screened by the atomic electrons. The differential cross section of such scattering was described by the Rutherford expression with a correction for the screening (Bethe, 1953):

$$\frac{d\sigma_y}{d\Omega} = Z^2 \frac{r_e^2}{\beta^2 p_e^2 (1 + 2\eta - \cos\theta)^2}, \tag{5}$$

where $d\Omega$ is a solid-angle element; p_e is the relativistic momentum of an electron in units of $m_e c$; η is the screening parameter; θ is the scattering angle. In the Thomas–Fermi model of an atom, the screening parameter is (Bethe, 1953; Zerby & Keller, 1967):

$$\eta = \left(\frac{Z^{1/3}}{137 \times 0.885} \right)^2 \frac{1.1 + 3.76(Z/137)^2 (T+1)^2/T(T+2)}{4T(T+2)}. \tag{6}$$

The following relationships were used in the above expression:

$$p_e^2 = T(T+2), \qquad \beta^2 = (v/c)^2 = T(T+2)/(T+1)^2.$$

The total energy losses were normalized in accordance with the Bethe–Bloch equation:

$$\frac{dT}{dS} = 0.3056 \frac{\rho Z}{A\beta^2} \left\{ \ln\left[\frac{T^2(T+2)}{2I^2} \right] + \frac{\frac{1}{8}T^2 + 1 - (2T+1)\ln 2}{(T+1)^2} \right\}, \tag{7}$$

where A and ρ are the atomic weight and the density of the gas, respectively; I is the average bond ionization potential, representing the average energy of an electron in an atom; its values, expressed in units of $m_e c^2$, were found from tabulated data or were calculated from the semiempirical Sternheimer expression:

$$I = \frac{Z(9.76 + 58.6 Z^{-1.10})}{0.511 \times 10^6}. \tag{8}$$

The described Monte Carlo algorithm was applied for the modeling of e-beam transportation from vacuum diodes into laser chamber throughout Al-Be and Ti foils. Figure 3 illustrates this process for the GARPUN laser by visualizing the trajectories of 100 individual electrons in a working gas at 1.5 atm pressure when the external magnetic field with 0.065 T inductance was switched off and on (the scale of the pictures in longitudinal direction is reduced 3.8 times). Note that typically in numerical modeling, the number of electrons reached 25,000–30,000. One could see clearly how the magnetic field confines the electrons, even though they are scattered during their passage through the foils and the gas. The Larmor radius for the electrons with an average

https://doi.org/10.1017/S0263034601194085 Published online by Cambridge University Press

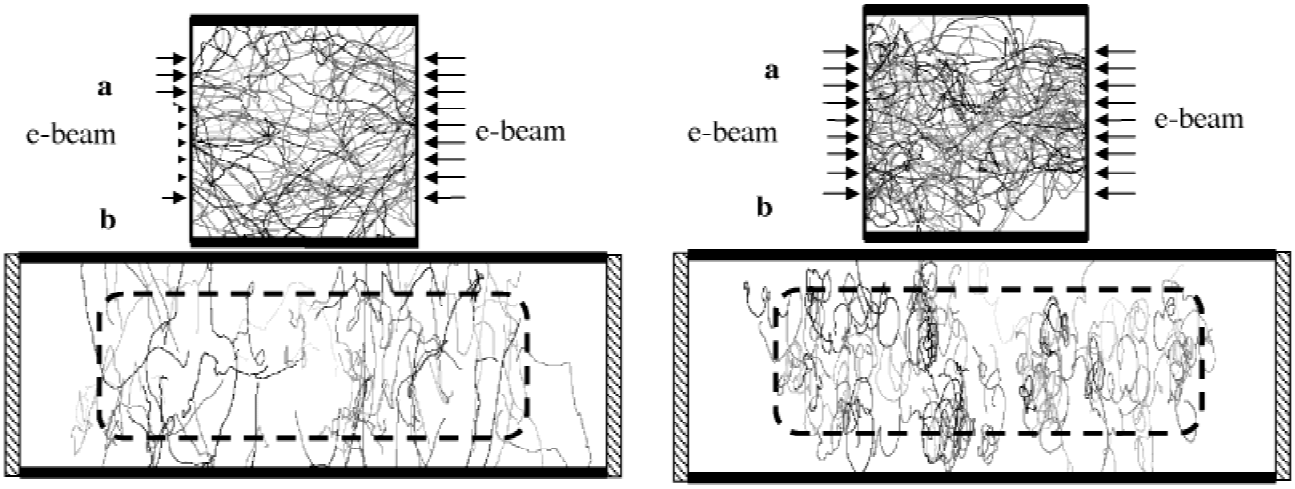

Fig. 3. Trajectories of individual electrons in the GARPUN laser chamber filled by 1.5-atm argon gas without (left) and with external magnetic field of 0.065 T (right). (a): View along laser axis. (b): View along e-beams (their initial cross section is shown by dotted line). The scale in the longitudinal direction is reduced 3.8 times.

energy $\varepsilon_e = 300$ keV is equal to $r_L = 3.3$ cm. The magnetic field significantly increases the density of electrons, and hence the specific pumping power in the central region of the laser chamber that corresponds approximately to an initial cross section of injected e-beams. At the same time, the total amount of particles reaching top and bottom walls as well as the laser windows is reduced. Thus the applied magnetic field controls not only energy losses due to scattered electrons, but also prevents the laser windows from illumination by energetic electrons.

4. E-BEAM TRANSPORT THROUGH Al-Be FOIL

This section presents the main results obtained in comparative studies of 50-μm thickness Al-Be and 20-μm Ti foils. Figure 4 demonstrates typical oscillograms of the current in the vacuum diode measured by the Rogowski coil (upper trace) and the current in the e-beam as measured by a Faraday cup located behind Al-Be foil (lower trace). Both signals have approximately the same FWHM of about 100 ns with the maximum current being reached at ~80 ns, but slightly different rise times. The latter might be caused by e-beam formation processes in the vacuum diode or lower electron energies in the beginning of the pulse. The e-beam current was $I_e = 10$ kA, which corresponded to an average value of current density $I_e/S_c \approx 50$ A/cm^2, where $S_c = 210$ cm^2 is the full area of the receiving plate of the Faraday cup. The e-beam absorption by the graphite was calculated with the Monte Carlo method to be 94–96% for electron energies in the range $\varepsilon_e = 200-600$ keV.

By varying the aperture (stop) in the Faraday cup, one can derive the distribution of current density across the width of the cathode (Fig. 5). The maximum value in the center is twice as high as the average value. This might be due to the geometry of the vacuum diode. It is also seen in Figure 5 that the external magnetic field did not significantly influence the electron beam current. This might be explained by the fact that the Faraday cup was set close to the foil, and hence would not be affected even with the mean scattering angles of 20–30° calculated for the expected electron energies of $\varepsilon_e = 300$–500 keV.

The transparency of the hibachi structure was determined by comparing the e-beam current through anode grid only (without hibachi or foil) against the current measured through the anode grid and hibachi (without foil). It was 83% if compared with 90% of geometric transparency. The differ-

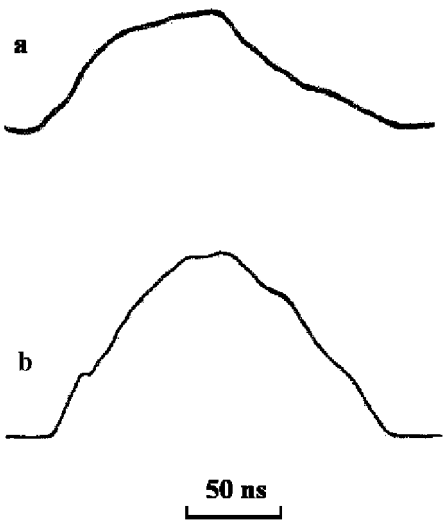

Fig. 4. Typical oscillograms of the current in vacuum diode (a) and e-beam current behind the foil (b).

https://doi.org/10.1017/S0263034601194085 Published online by Cambridge University Press

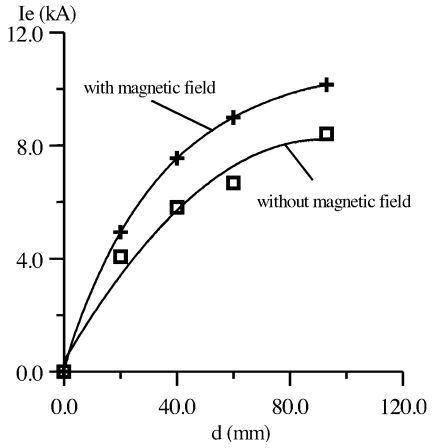

Fig. 5. E-beam currents versus opened gap width.

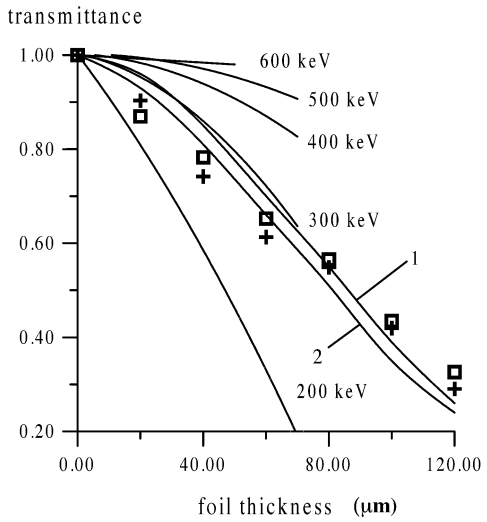

Fig. 6. Experimental transmittance in dependence on thickness of Ti foils and numerical calculations for monoenergetic electrons with $\varepsilon_e = 200–600$ keV, e-beams with uniform energy distribution in $\varepsilon_e = 250–350$ keV range and input e-beam divergence $\Delta\alpha = 0°$ (1) or $\Delta\alpha = 45°$ (2).

ence was apparently due to the transverse component of electron velocity.

The transport of the initial e-beam generated in vacuum diode through the foils, either Al-Be or Ti, was found by directly comparing measurements of the electron beam current behind the full hibachi (i.e., anode grid, hibachi structure, and foil) with those obtained with just the grid and hibachi structure. Within a measurement accuracy of 5%, both Al-Be and Ti foils demonstrated equal transmittance of 75%. However these measured values are significantly less than the calculated value of 100 to 91% when electron energy was varied from 400 down to 200 keV. We suppose that this discrepancy might be originating from a wide energy distribution of electrons in the initial e-beam generated in the vacuum diode. If indeed there are low energy electrons that are stopped in the foil, this is undesirable not only because they lower the transmission efficiency, but also because they heat the foil, which may lead to premature foil failure in a repetition-rate laser facility.

Experiments have been performed to measure the energy distribution of the electrons at the entrance into laser chamber after the e-beam passes throughout the Al-Be (or Ti) foil. In this case, the e-beam current was measured as a function of the total thickness of additional Ti foils set between the main foil and the Faraday cup. These results are shown in Figure 6 together with the calculated ones. The approximately linear decrease in the transmitted current with foil thickness cannot be explained by any calculated dependence for monoenergetic electrons with the energies between $\varepsilon_e = 200$ and $\varepsilon_e = 600$ keV. On the other hand, good agreement with the data can be achieved if it is assumed that the electron energies were distributed uniformly in the range $\varepsilon_e = 250–350$ keV ($\Delta\varepsilon_e = 100$ keV), having a mean value $\langle\varepsilon_e\rangle = 300$ keV. Different angular distributions $\Delta\alpha = 0°$ (1) and $\Delta\alpha = 45°$ (2) of initial electron velocities in the e-beam before the foil have been compared and they demonstrated small influence on the transmittance.

5. STATISTICS AND MORPHOLOGY OF Al-Be FOIL DAMAGE

We did not achieve the fatal damage of Al-Be foils in either the preamplifier (550 pulses) nor amplifier modules (1000 e-beam pulses). This is significantly higher than the mean lifetime of Ti foils. After these series, both types of foils were examined visually with an optical microscope. No noticeable changes were observed on the Al-Be foil surface after a protracted fluorine action, even if the foil sample was then taken into atmospheric air. This is clearly seen in the microscope pictures of Al-Be foil presented in Figure 7a,b. Both sides of the foil, that is, both laser and diode sides, look identical. It would seem that the most likely cause for the long life behavior is the formation of AlF_3 on the surface of the foil, which is stable against further fluorine contamination. The only visible defects on the Al-Be foil surface were spread with an average density of 1–2 per 100 cm^2 and looked from the vacuum diode side (Fig. 7a) as microcraters with a nonthrough hole in a center surrounded by a rim of ejected material. They were also accompanied by a halo of thermal burn. These nonfatal defects might have originated from the impacts of charged microparticles of the cathode material accelerated by an electric field or micropinched discharges inside vacuum diode. It should be noted that cathodes after prolonged operation also demonstrated thermal burn spots spread casually across their surfaces. But they had a rather bigger diameter of about a centimeter. The micropicture of the backside of the same Al-Be foil sample is shown in Figure 7b. This image has been mirrored using the same axis that the foil was rotated about. It allows one to make more precise comparison of both sides of the foil. For example, it is clearly seen that the laminating Al layer of

https://doi.org/10.1017/S0263034601194085 Published online by Cambridge University Press

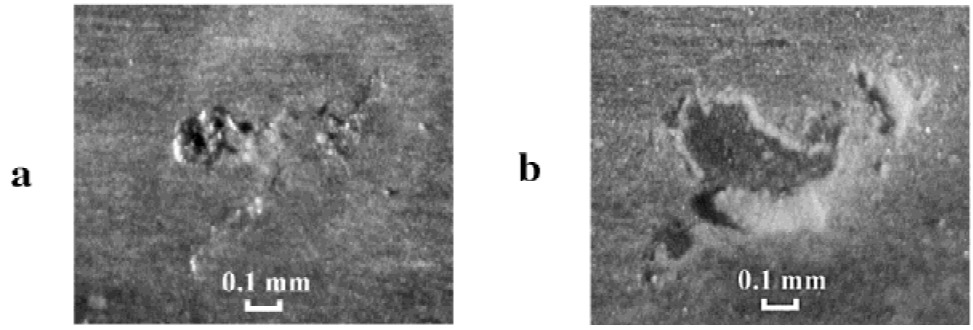

Fig. 7. Microscopic pictures of Al-Be foil after multiple e-beam irradiation in fluorine-containing working gas mixture of KrF laser. (a): Foil surface from a side of vacuum diode. (b): The same area from a side of laser cell (mirror-converged image).

2-μm thickness was spalled exactly opposite the microcraters. The spallation effect was apparently caused by a shock wave that was generated in a foil by the microparticle impacts or local energy release in the micropinches. Therefore the initial layered structure of Al-Be foil seems to be more reliable in regard to short-pulse mechanical breakdown than monolayer foil.

In marked contrast to the Al-Be, the Ti foils did not survive so well. The side of the foil facing the laser gas showed a friable material of dark-red, violet, or white color. TiF_3 and TiF_4, substances being the most probable in the chemistry of Ti and F, are not stable with the temperature and could not protect the rest of the foil, consequently. In addition, they would absorb water vapor from the air. As a result, a large amount of through holes arose in the Ti foil some time later even after short existence in the air. Apparently, it was due to a strong action of HF acid that might be formed between absorbed H_2O and F. Figure 8 illustrates these outcomes for Ti foil, where serious degradation of the foil surface and a formation of a typical through hole are clearly observed.

6. DISTRIBUTION OF SCATTERED ELECTRONS IN LASER CHAMBER

The distribution of the energy fluence of e-beams and of scattered electrons has been measured by means of calorimeters located throughout the GARPUN laser chamber (see Fig. 2a). One of them (10) had an open graphite receiving plate of 5-cm diameter and directly measured the energy of the incoming e-beam. Another calorimeter of 2.7-cm diameter was placed at different positions (11, 12) along the chamber axis outside the e-beam path. A 20-μm-thick aluminized polymer film was placed in front of the calorimeter to diminish heat and radiation fluxes due to temperature rise and argon fluorescence during e-beam deposition. The calorimeter was oriented perpendicular to the e-beam axis (along the laser axis) so it measured only the scattered electrons (and a small amount of soft X rays that might be absorbed by its $\sim$200-μm-thick copper receiving plate). Heat transfer from the gas was taken into account by subtracting the successive value obtained when the calorimeter was turned in the opposite direction. The indicated energies were then multiplied by the coefficient 2.2, which accounted for the full aperture angle of the calorimeter of 84° in assumption that scattered electrons were uniformly distributed in a solid angle of 2π sr. Numerical calculations using the Monte Carlo code confirmed this correction procedure.

Figure 9 gives the energy fluence delivered by each of the two e-beams to the middle point of the laser chamber as a function of the buffer argon gas pressure and guiding magnetic field. It is seen that the magnetic field strongly influences the electron beam transport from the vacuum diodes into the laser chamber. In our previous experiments, electron beam pinching took place without a magnetic field.

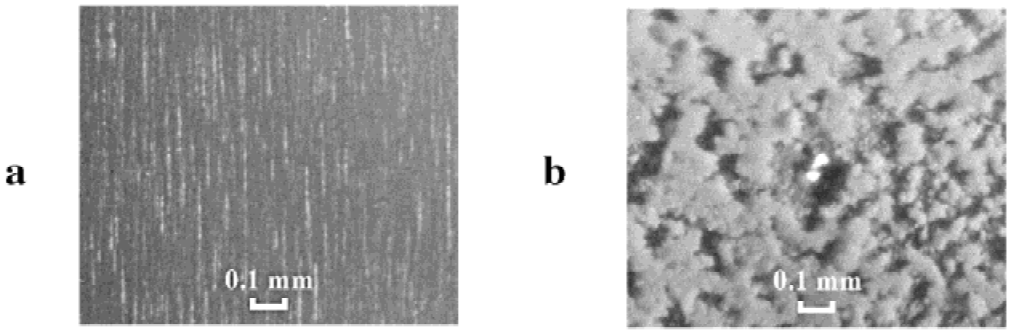

Fig. 8. Microscopic pictures of Ti foils before (a) and after (b) multiple e-beam irradiation in fluorine-containing working gas mixture of KrF laser. (b): View from a side of the laser cell.

https://doi.org/10.1017/S0263034601194085 Published online by Cambridge University Press

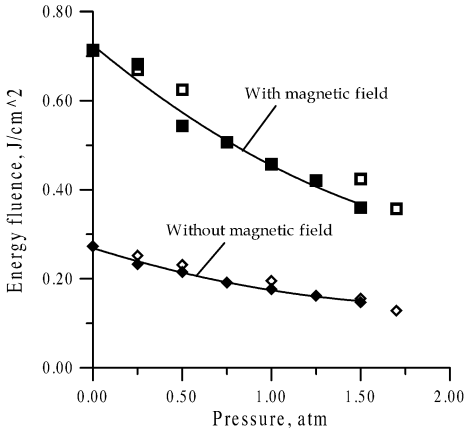

Fig. 9. Dependence of energy fluence for one e-beam in the middle of the laser chamber on argon pressure with and without a magnetic field. Solid dots: experiments; outlined dots: calculations.

This would introduce additional losses and scattering of electrons (Basov *et al.*, 1993; Bakaev *et al.*, 1994). Such an effect is clearly demonstrated in Figure 10, where the energy fluence of scattered electrons at 8.5-cm distance from the electron beam boundary was much higher without the magnetic field than with the field. When the distance was doubled to 17 cm, the energy fluence was significantly lower, especially at higher gas pressure. As a result, we could not detect the scattered electrons in the presence of the magnetic field at all.

A comparison of the experimental results on e-beam scattering (1) with the numerical modeling (2) in Figure 10 reveals a great discrepancy at low argon pressures, if only e-beam scattering in the foils and in the gas was assumed. Although a low-pressure range is untypical for KrF laser pumping conditions, it stimulated us to look for some additional effects. Multiple passages of electrons from one vacuum diode into the laser chamber, then into another vacuum diode, and then once again in the opposite direction were considered. This might take place at higher gas pressures, but only if one makes the electron energy too high in order to make uniform a specific pumping power across laser chamber. In this multipassage case, a mean scattering angle would increase and additional significant heat loading of the foils would appear due to absorption of decelerated electrons. It is also possible that the scattering might be caused by e-beam interaction with the hibachi structure particularly without magnetic field guiding. Both these effects were taken into account (the latter by introducing an angular distribution of initial e-beams with $\Delta\alpha = 45°$) in the next run of calculations (3) that demonstrates good qualitative agreement with experimental results (1) in Figure 10.

The same assumptions have been made to calculate the distribution of scattered electrons along the axis of the laser chamber at typical argon pressure of 1.5 atm (Fig. 11). The distance in this graph is measured from the boundary of the initial e-beams (cathode edge). The two experimental points coincide well with calculated ones. The main conclusion to be drawn from these investigations is that the external magnetic field, besides increasing pumping efficiency and uniformity, strongly reduces electron bombardment of the laser windows.

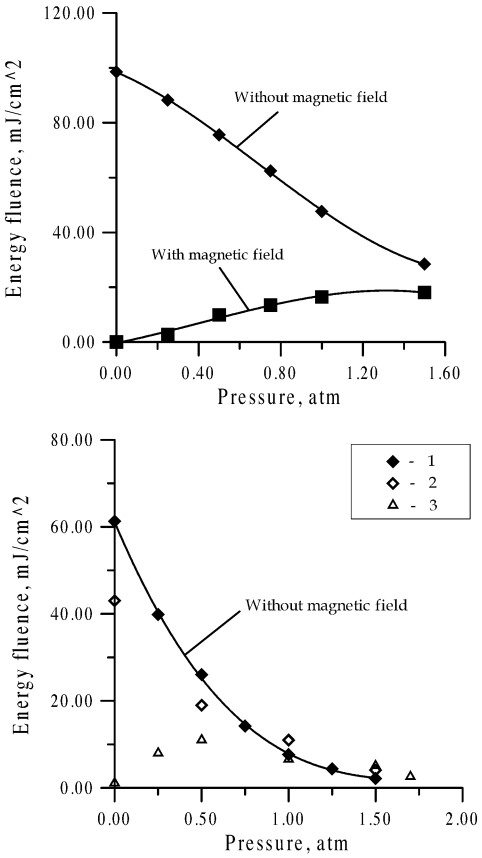

Fig. 10. Energy fluence of scattered electrons in dependence on argon pressure at 8.5-cm (top) and 17-cm distance (bottom) from e-beams. 1: experiments; 2,3: calculations.

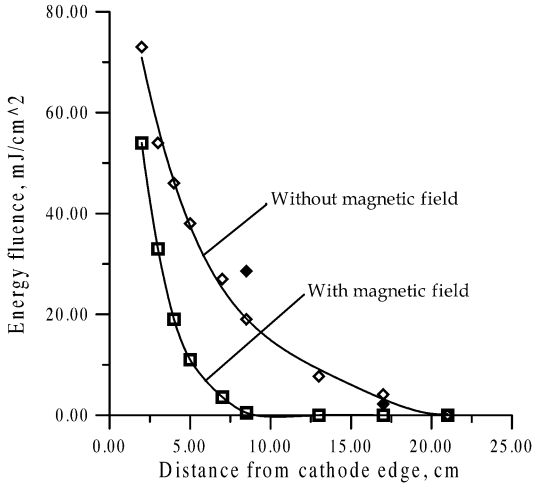

Fig. 11. Distribution of scattered electrons along the axis of the laser chamber at an argon pressure of 1.5 atm. Solid dots: experiments, outlined dots: calculations.

https://doi.org/10.1017/S0263034601194085 Published online by Cambridge University Press

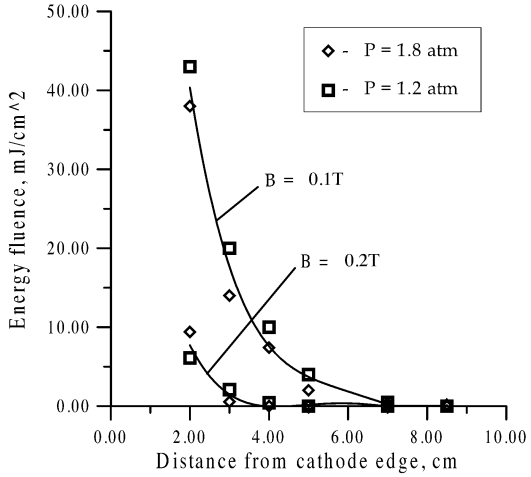

Fig. 12. Distribution of scattered electrons along the axis of the laser chamber for NRL repetition-rate ELECTRA laser conditions.

The Monte Carlo code has also been applied to simulate analogous distributions for the NRL repetition-rate ELECTRA laser. It has an active volume of 30 × 30 × 100 cm pumped by two opposite-side 500 keV, 112 kA, 100-ns e-beams stabilized by the magnetic field (Sethian *et al.*, 1998, 1999). The calculated distributions of scattered electrons along the axis of the laser are shown in Figure 12 for various working gas pressures and magnetic field values. It is clearly seen that the amount of scattered electrons falls down rapidly with increasing magnetic field. Gas pressure being varied in the optimal pumping range does not significantly affect the electron scattering.

7. INVESTIGATION OF E-BEAM-INDUCED ABSORPTION IN CaF_2 WINDOWS

Both transient and residual e-beam-induced absorption in CaF_2 samples set into laser chamber have been investigated. Their initial transmittance was measured by means of a spectrophotometer to be in the range of 91.5–92.3%, which corresponded very closely to Fresnel reflection by both sides of the plates.

7.1. Transient induced absorption

Figure 2b gives the layout of e-beam-induced transient absorption measurements. The 10-mm-thick CaF_2 plates under investigation were inserted inside the laser chamber at different positions (10, 11, 12) relative to the incoming e-beams and were transmitted by a probe radiation with $\lambda =$ 248-nm wavelength and 0.1 MW/cm^2 intensity. The probe radiation was generated by a discharge-pumped KrF laser, which was synchronized with the e-beams by means of a laser-driven switch in the high-voltage power supply of vacuum diodes. Either thin aluminum coating on the back surface of the sample (11, 12) or an additional mirror (13) outside the laser chamber reflected the probe radiation. Thus in both cases, the radiation twice passed through the tested plate and was attenuated due to the induced absorption. Both input and output laser pulses of ~25 ns FWHM duration were measured with two vacuum photodiodes (14, 15). They were both recorded on the same oscilloscope channel by inserting a small time delay in one of them (Fig. 13a). The synchronization of the e-beam pulse with the probe radiation pulses was established by simultaneous registration of the current pulse in one of the pulse-forming lines as measured by a low-inductance shunt. Fluorescence of the excited argon gas that filled the laser chamber was measured by the third photodiode (16). Both the current and fluorescence pulses had similar waveforms as shown in Figure 13b,c.

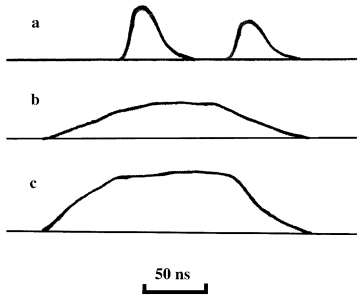

Fig. 13. Typical oscillograms of input and output probe laser pulses (a), argon fluorescence (b), and current in the forming line (c).

When the CaF_2 sample was tested at the position (10) it was necessary to account for absorption of probe radiation in the excited argon gas in front and behind the plate. The argon pressure was varied up to 1.6 atm, which is a typical value for large-scale KrF lasers. Figure 14 gives the argon transmittance (for two passes) as a function of pressure during e-beam pumping both with and without a magnetic field. Significantly increased e-beam current density under magnetic field guiding (see Fig. 9) led to higher argon excitation and correspondingly lowered its transmittance. The net induced transmittance of the CaF_2 plate turned by an

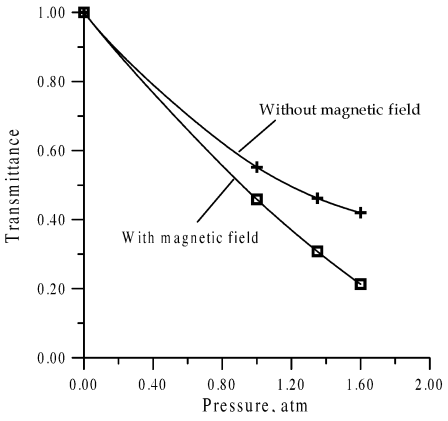

Fig. 14. Argon transmittance in dependence on gas pressure.

https://doi.org/10.1017/S0263034601194085 Published online by Cambridge University Press

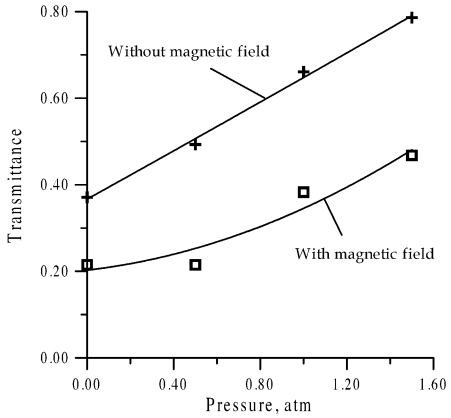

Fig. 15. Transmittance of CaF_2 sample set in the middle of the laser chamber in dependence on argon pressure.

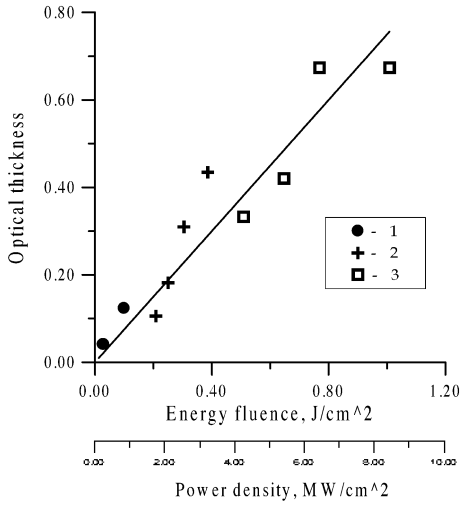

Fig. 16. Dependence of optical thickness of transient induced absorption in CaF_2 on specific power density (energy fluence) of scattered electrons (1), or injected e-beams without (2) and with guiding magnetic field (3).

angle of 45° to incoming e-beams and probe radiation is shown in Figure 15. The transmittance increased with the argon pressure, and was also higher without the magnetic field. This is as expected, as the e-beams were more absorbed in a gas at higher pressures and more scattered without a magnetic field.

The tested sample was displaced along the chamber axis and set in turn at 8.5 cm and 17 cm outside the region that was directly irradiated by e-beams (that approximately corresponded to the emitting area of the cathodes) so that only scattered electrons and X rays could interact with it. In this case, another optical scheme was used for measurements. To eliminate absorption of probe radiation in the excited argon and thus to increase the sensitivity and accuracy of measurements, the back surface of the sample was coated by a 1-μm-thick aluminum layer reflecting probe radiation. We did not measure any noticeable induced absorption in the CaF_2 plate, which was set at 17 cm away from the electron beam boundary either with a magnetic field or without it. When the sample was set at a half of this distance, a small drop in CaF_2 transparency was detected only with no magnetic field. At typical argon pressure of $p = 1.5$ atm, the relative transient transmittance averaged over 10 shots was $T = 0.92 \pm 0.06$. It decreased slightly at lower argon pressures.

Optical densities (thickness) of transient induced absorption Δ in CaF_2 samples are compared with specific power densities P of e-beam irradiation in Figure 16. The variety of experimental results obtained in the middle of the laser chamber (sample position 10 in Fig. 2b) is completed by two measurements for sample position 11. The Δ values derived from relative transmittance measurements in Figure 15 account for an oblique incidence of e-beams and probe laser radiation onto the sample at the angle of 45°. Specific power densities $P = \varepsilon/\tau$, where ε is the energy fluence of electrons, τ = 120-ns pulse duration, were found from the data in Figures 9 and 10. The variety of experimental dots in Figure 16 could be approximated by a linear dependence $\Delta = kP$, where coefficient of proportionality $k = 90 \pm 25$ cm^2/GW was close to that obtained earlier (Barabanov & Sergeev, 1995).

7.2. Residual induced absorption

To measure the residual induced absorption in the CaF_2 samples, they were set at the same positions inside the laser chamber as in the transient absorption measurements. A 20-shot train was carried out with the magnetic field on. In the case where the samples were turned perpendicular to the electron beams, the total energy fluence was $\varepsilon_\Sigma \sim 16$ J/cm^2. The absolute transmittance of CaF_2 (including Fresnel reflection) measured by spectrophotometer immediately after irradiation decreased down to 86%. The sample placed 8.5 cm away from the electron-beam boundary, and rotated to look at just scattered electrons, was exposed to a fluence of $\varepsilon_\Sigma \sim 0.15$ J/cm^2, and had a residual transmittance of 89%. So the residual optical density was reduced slower than the electron fluence. This showed that, in the latter case, the residual absorption might be caused by something else in addition to electrons, for example, by X-ray irradiation. It should be noted that absolute transmittance of CaF_2 output windows of the GARPUN laser, which were ~20 cm far away from e-beams boundary and which have suffered several thousands shots during last five years, remain continuously at the level of 90%.

8. ANALYSIS OF LIMITATIONS DUE TO X-RAY-INDUCED ABSORPTION

The results discussed above give evidence that proper design of the laser chamber and applied magnetic field allow one to avoid difficulties with e-beam-induced absorption in the output windows. The distance to the windows should be

https://doi.org/10.1017/S0263034601194085 Published online by Cambridge University Press

determined by the compromise between losses of laser radiation in the unpumped region of a gas due to molecular fluorine absorption and electron escape onto the windows. The last can be reduced significantly in a magnetically confined pumping geometry. In addition to fused silica, CaF_2 windows might be used successfully due to their resistance to fluorine and low nonlinear absorption coefficient. But even in the absence of scattered electrons, there is some risk of transparency degradation for both materials due to bremsstrahlung X-ray radiation that accompanied deceleration of energetic electrons when they pass through the foil unit and gas in the laser chamber. In accord with experimental practice and existing theoretical representations, different kinds of ionizing radiation are practically identical in modification of optical materials, if they act through the electronic subsystem (Jones *et al.*, 1989; Lushchik & Lushchik, 1989; Williams, 1989). It manifests in accumulating color centers during relaxation of electron-hole pairs. The resulting induced absorption in optical materials would be determined only by the aggregate absorbed dose or by the introduced specific power. However, an exposure by e-beam with electron energy $\geq$200 keV, energy density $\geq$1 J/cm^2, and with pulse-width of $\sim$100 ns (as in our experiments) may cause an additional mechanism for defects formation, such as knocking out atoms or ions from the sites of the lattice. This would give a large concentration of electronic excitations in the near-surface stratum that might cause nonlinear mechanisms of defect formation, for example, a recombination of two excitons. It is not clear yet what mechanism was responsible for induced absorption in present experiments, and therefore, X rays and energetic electrons are equivalent in regard to induced absorption at the same exposure doses. More investigations are needed to answer these questions. They should include *in situ* measurements of induced absorption at prolonged X-ray irradiation of samples simultaneously with an action of intensive laser radiation. The latter might increase or decrease a rate of absorbing centers production in different ionic crystals if compared with only X-ray irradiation (Sergeev, 1995). The data concerning ionizing radiation resistance of fused silica are available (Tohmon *et al.*, 1989), but the simultaneous action of laser and ionizing radiation should be investigated as well.

Accurate measurements of the X-ray yield from the laser module also should be done. The scaling formula for energy fluence of X rays incident onto laser windows was derived earlier (Barabanov *et al.*, 1992):

$$\varepsilon_X = C_X(ZE_L^s W^2), \tag{9}$$

where C_x is the coefficient proportionality; Z is the nuclear charge of atoms in the matter, which decelerates the e-beam; E_L is laser energy; W is the specific pumping power, s is a coefficient weakly dependent on E_L and the laser geometry (usually it has a value of $\sim$1.5). This scaling law should be verified experimentally and coefficient C_x should be determined.

8. CONCLUSIONS

Experiments have been performed with the single-pulse large-aperture e-beam-pumped GARPUN KrF laser installation to investigate high-current e-beam transport through aluminum-beryllium foil, its lifetime for multiple e-beam irradiation, as well as its reaction to protracted fluorine action. E-beam scattering in the laser chamber in typical pumping conditions with and without a guiding magnetic field was also investigated. E-beam-induced absorption of laser radiation in calcium fluoride optical windows has been measured. Both problems are related to the development of durable and efficient repetition-rate KrF laser drivers for inertial fusion energy.

The main results obtained during the present investigation are as follows.

1. A large-aperture GARPUN module with 16 $\times$ 18 $\times$ 100 cm active volume pumped by two-side counterpropagating e-beams and a middle-aperture BERDYCH module with a single-side-pumped active volume of 10 $\times$ 10 $\times$ 100 cm were adjusted for e-beam transport and Al-Be foil lifetime investigations. Both modules used a magnetic field to guide e-beams with an average electron energy of $\sim$300 keV and a current density of $\sim$50 A/cm^2 from vacuum diodes into laser chamber.
2. A Monte Carlo numerical code has been developed to calculate e-beam transport through different foil materials and distribution of scattered electrons inside the laser chamber.
3. The transparency of 50-μm-thick Al-Be foil and 20-μm Ti foil has been compared for 300 keV e-beams using Faraday cups. Both foils demonstrated equal transmittance of 75%, but this was lower than calculated. The discrepancy was apparently due to the presence of low-energy electrons in the initial e-beam.
4. No fatal damages and no surface modification due to fluorine etching were observed for Al-Be foils at GARPUN and BERDYCH modules after 1000 and 550 e-beam shots. It had significantly higher lifetime than Ti foils in the same conditions.
5. Distribution of scattered electrons has been measured by calorimeters for the GARPUN laser. It was shown that an applied magnetic field of $\sim$0.1 T significantly reduced the energy fluence of scattered electrons that affected the transparency of laser windows.
6. A Monte Carlo code, being tested with the GARPUN laser, has been applied to simulate e-beam scattering in the NRL repetition-rate ELECTRA laser.
7. Transient absorption in CaF_2 windows induced by fast electrons being measured in comparison with distribution of scattered e-beams revealed linear dependence between induced optical thickness and specific power density of e-beam irradiation. The residual absorption

https://doi.org/10.1017/S0263034601194085 Published online by Cambridge University Press

was determined by some additional factors, that is, X-ray irradiation.

8. Optimization of any e-beam-pumped KrF laser module should be done in compromise between absorption in unpumped region and optical windows.

ACKNOWLEDGMENTS

We are grateful to E.V. Polyakov for the assistance in experiments, and to J. Sethian from the Naval Research Laboratory for useful discussions. This work was supported by the Naval Research Laboratory under Contract No. N68171-99-M-6338.

REFERENCES

Amosov, A.V., Barabanov, V.S., Gerasimov, S.Yu., Morozov, N.V. & Sergeev, P.B. (1993). Electron-beam-induced absorption of laser radiation in a quartz glass at wavelengths 193, 248, and 353 nm. *Quant. Electron.* **23**, 939–942.

Arlantsev, S.V., Grigor'yants, E.A., Vadkovskii, A.D., Zvorykin, V.D. & Metreveli, G.E. (1994). Pumping of the GARPUN wide-aperture excimer laser by counterpropagating electron beams. *Quant. Electron.* **24**, 223–228.

Bakaev, V.G., Vadkovskii, A.D., Danilov, E.O., Grigor'yants, E.A., Zvorykin, V.D., Metreveli, G.E. & Sychugov, G.V. (1994). Generation of electron beams for pumping of the GARPUN wide-aperture excimer laser. *Quant. Electron.* **24**, 5–12.

Barabanov, V.S., Morozov, N.V. & Sergeev P.B. (1992). Ionizing radiation induced absorption in KrF-laser windows. *J. Non-crystalline Solids* **149**, 102–106.

Barabanov, V.S. & Sergeev, P.B. (1995). Electron-beam-induced absorption of ArF, KrF, and XeF laser radiation in optical materials. *Quant. Electron.* **25**, 717–720.

Basov, N.G., Bakaev, V.G., Bogdanovskii, A.V., Vadkovskii, A.D., Grigor'yants, E.A., Zvorykin, V.D., Metreveli, G.E., Suchkov, A.F. & Sychugov, G.V. (1993). E-beam pumped "Garpun" broadband KrF Laser with ~1GW Pulsed Lasing Power. *J. Sov. Laser Res.* **14**, 326–359.

Basov, N.G., Bakaev, V.G., Grigor'yants, E.A., Danilov, E.O., Zvorykin, V.D., Kobelev, P.V., Metreveli, G.E., Polyanskii, S.V., Proleiko, I.V., Suchkov, A.F. & Sychugov, G.V. (1991). Wide-aperture electron-beam-pumped excimer KrF laser with an output power of 1 GW. *Sov. J. Quant. Electron.* **21**, 816–817.

Bethe, H.A. (1953). Moliere's theory of multiple scattering. *Phys. Rev.* **89**, 1256.

Divall, E.J., Edwards, C.B., Hirst, G.J., Hooker, C.J., Kidd, A.K., Lister, J.M.D., Mathumo, R., Ross, I.N., Shaw, M.J., Toner, W.T., Visser, A.P. & Wyborn, B.E. (1996). Titania- a 10^{20} Wcm^{-2} ultraviolet laser. *J. Mod. Opt.* **43**, 1025–1033.

Divall, E.J. & Hirst, G.J. (1993). Radiation damage to Goblin windows. In Report RAL-93-031, Oxfordshire, UK: Rutherford Appleton Laboratory, p. 143.

Divall, E.J., Hirst, G.J., Lister, J.M.D. & Mathumo, R. (1995). Sprite operations. In Report 1994-5 RAL-TR-95-025, Oxfordshire, UK: Rutherford Appleton Laboratory, p. 119.

Eliseev, E.N., Fadeeva, E.I., Zvorykin, V.D., Morozov, N.V., Sagitov, S.I. & Sergeev, P.B. (1996). Laser strength of optical materials and coatings for ArF and KrF excimer lasers. *J. Opt. Technol.* **63**, 136–143.

Grigorev, Y.V. & Stepanov, A.V. (1990). Separating membranes for exit windows of electron guns. *Instrum. Exper. Techniq.* **33**, 895.

Harris, D.B., Allen, G.R., Berggren, R.R., Cartwright, D.C., Czuchlewski, S.J., Figueira, J.F., Hanson, D.E., Hauer, A., Jones, J.E., Kurnit, N.A., Leland, W.T., Mack, J.M., Mcdonald, T.E., Mcleod, J., Rose, E.A., Sorem, M., Sullivan, J.A. & Watt, R.G. (1993). Strengths and weaknesses of KrF lasers for inertial confinement fusion applications learned from the AURORA laser. *Laser Part. Beams* **11**, 323–330.

Hunter, A.M., Hunter, R.O. & Johnson, T.H. (1986). Scaling of KrF lasers for inertial confinement fusion. *IEEE J. Quant. Electron.* **QE-22**, 386–404.

Jones, S.C., Braunlich, P., Kasper, R.T., Chen, X. & Kelly, P. (1989). Recent progress on laser-induced modifications and intrinsic bulk damage of wide-gap optical materials. *Opt. Eng.*, **28**, 1039–1067.

Krajnovich, D.J., Kulkarni, M., Leung, W., Tam, A.C., Spool, A. & York, B. (1992). Testing of the durability of single-crystal calcium fluoride with and without antireflection coatings for use with high-power KrF excimer lasers. *Appl. Opt.* **31**, 6062–6075.

Lowenthal, D.D., Ewing, J.J., Center, R.E., Mumola, P.B., Grossman, W.M., Olson, N.T. & Shannon, J.P. (1981). Conceptional design of an angular multiplexed 50 kJ KrF amplifier for ICF. *IEEE J. Quant. Electron.* **QE-17**, 1861–1870.

Lushchik, Ch.B. & Lushchik, A.Ch. (1989). *Decay of Electronic Excitations with Defect Formation in Solids.* Moscow: Nauka (in Russian).

McGeoch, M.W., Corcoran, P.A., Altes, R.G., Smith, I.D., Bodner, S.E., Lehmberg, R.H., Obenschain, S.P. & Sethian, J.D. (1997). Conceptual design of a 2 MJ KrF laser facility. *Fusion Technol.* **32**, 610–643.

Obenschain, S.P., Bodner, S.E., Colombant, D., Gerber, K., Lehmberg, R.H., Mclean, E.A., Mostovych, A.N., Pronko, M.S., Pawley, C.J., Schmitt, A.J, Sethian, J.D., Serlin, V., Stamper, J.A., Sullivan C.A., Dahlburg, J.P., Gardner, J.H., Chan, Y., Deniz, A.V., Hardgrove, J., Lehecka, T. & Klapisch, M. (1996). The Nike KrF laser facility: Performance and initial target experiments. *Phys. Plasmas* **3**, 2098–2107.

Owadano, Y., Okuda, I., Matsumoto, Y., Matsushima, I., Koyama, K., Tomie, T. & Yano, M. (1993). Performance of the ASHURA KrF laser and its upgrading plan. *Laser Part. Beams* **11**, 347–351.

Owadano, Y., Okuda, I., Matsumoto, Y., Tanimoto, M., Tomie, T., Koyama, K. & Yano, M. (1989). Development of a high-power Krf laser system, ASHURA. *Laser Part. Beams* **7**, 383–392.

Owadano, Y., Okuda, I., Yashiro, E., Matsushima, I., Matsumoto, Y., Miura, E., Tomie, T. & Takahashi, E. (1996). Super-ASHURA KrF laser development. In *Proc. 15th Int. Conf. on Plasma Physics and Controlled Nuclear Fusion Research*, Seville, Spain, September–October 1994, Vol. 3, pp. 121–127. Vienna: International Atomic Energy Agency.

Pawley, C.J., Gerber, K., Lehmberg, R.H., McLean, E.A., Mostovych, A.N., Obenschain, S.P., Sethian, J.D., Serlin, V., Stamper, J.A., Sullivan, C.A., Bodner, S.E., Colombant, D., Dahlburg, J.P., Schmitt, A.J., Gardner, J.H., Brown, C., Seely, J.F., Lehecka, T., Aglitskiy, Y., Deniz,

A.V., Chan, Y., Metzler, N. & Klapisch, M. (1997). Measurements of laser-imprinted perturbations and Rayleigh-Taylor growth with Nike KrF laser. *Phys. Plasmas* **4**, 1969–1977.

Rosocha, L.A., Bowling, P.S., Burrows, M.D., Kang, M., Hanlon, J., McLeod, J. & York, G.W. Jr. (1986). An overview of Aurora: A multi-kilojoule KrF laser system for inertial confinement fusion. *Laser Part. Beams* **4**, 55–70.

Rosocha, L.A., Hanlon, J.A., McLeod, J., Kang, M., Kortegaard, B.L., Borrows, M.D. & Bowling, P.S. (1987). Aurora Multikilojoule KrF laser system prototype for inertial confinement fusion. *Fusion Technol.* **11**, 497–531.

Rosocha, L.A. & Riep, K.B. (1987). Electron-beam sources for pumping large aperture KrF lasers. *Fusion Technol.* **11**, 576–611.

Sasaki, A., Ueda, K., Takuma, H. & Kasuya, K. (1989). Amplified spontaneous emission in high power KrF lasers. *J. Appl. Phys.* **65**, 231–236.

Sergeev, P.B. (1995). Avalanche-type mechanisms of ionic crystal destruction at UV and VUV laser radiation influence. *Bull. Lebedev Phys. Inst.* **5**, 39–45.

Sethian, J.D., Obenschain, S.P., Gerber, K.A., Pawley C.J., Serlin, V., Sullivan C.A., Webster, W., Deniz, A.V., Lehecka, T., McGeoch, M.W., Altes, R.A., Corcoran, P.A., Smith, I.D. & Barr, O.C. (1997a). Large area electron beam pumped krypton fluoride laser amplifier. *Rev. Sci. Instrum.* **68**, 2357–2366.

Sethian, J.D., Obenschain, S.P., Lehmberg, R.H. & McGeoch, M.W. (1998). KrF lasers for inertial fusion energy. In *Proc. 17th IEEE/NPSS Symposium on Fusion Engineering*, San Diego, CA, October 1997, pp. 593–597. Piscataway, NJ: IEEE.

Sethian, J.D., Obenschain, S.P., Lehmberg, R.H. & McGeoch, M.W. (1999). A rep-rate KrF system to address the issues relevant to inertial fusion energy. *Fusion Engg. Design* **44**, 371.

Sethian, J.D., Pawley C.J., Obenschain, S.P., Gerber, K.A., Serlin, V., Sullivan C.A., Lehecka, T., Webster, W., McGeoch, M.W., Smith, I.D., Corcoran, P.A. & Altes, R.A. (1997b). The Nike electron-beam-pumped KrF laser amplifiers. *IEEE Trans. Plasma Sci.* **25**, 221–228.

Shaw, M.J. (1991). Prospects for high-power KrF lasers. *Laser Part. Beams* **9**, 309–328.

Shaw, M.J., Bailly-Salins, R., Edwards, B., Harvey, E.C., Hooker, C.J., Key, M.H., Kidd, A.K., Lister, J.M.D. & Ross, I.N. (1993). Development of high-performance KrF and Raman laser facilities for inertial confinement fusion and other applications. *Laser Part. Beams* **11**, 331–346.

Shaw, M.J., O'Neil, F., Edwards, C.B., Nicholas, D.J. & Craddok, D. (1982). Sprite-A 250 J KrF laser. *Appl. Phys. B* **28**, 127.

Smiley, V.N. (1990). Review of high power excimer lasers. In *SPIE Proceedings* **1225**, pp. 2–9.

Sviatoslavsky, I.N., Sawan, M.E., Peterson, R.R., Kulcinski, G.L., MacFarlane, J.J., Wittenberg, L.J., Khater, H.Y., Mogahed, E.A. & Rutledge, S.C. (1992). A KrF laser driven inertial fusion reactor "Sombrero." *Fusion Technol.* **21**, 1470–1474.

Sullivan, J.A. (1987). Design of a 100-kJ KrF power amplifier module. *Fusion Technol.* **11**, 684–704.

Sullivan, J.A., Allen, G.R., Berggren, R.R., Czuchlewski, S.J., Harris, D.B., Jones, M.E., Krohn, B.J., Kurnit, N.A., Leland, W.T., Mansfield, C., McLeod, J., Mccown, A.W., Pendergrass, J.H., Rose, E.A., Rosocha, L.A. & Thomas, V.A. (1993). KrF amplifier design issues and application to inertial confinement fusion system design. *Laser Part. Beams* **11**, 359–383.

Sullivan, J.A. & von Rosenberg, C.W. Jr. (1986). High energy krypton fluoride amplifiers for laser-induced fusion. *Laser Part. Beams* **4**, 91–105.

Swingle, J.C., Schlitt, L.G., Rapaport, W.R., Goldhar, J. & Ewing, J.J. (1981). Efficient narrowband electron beam pumped KrF laser for pulse-compression studies. *J. Appl. Phys.* **52**, 91–96.

Takahashi, E., Okuda, I., Matsumoto, Y., Kato, S., Kuwahara, K. & Owadano, Y. (1999). Electron-beam pumped high-repetition rate KrF laser system. In *Book of Abstracts of International Forum on Advanced High-Power Lasers and Applications AHPLA' 99*, Osaka, Japan, 1–5 November, paper 3886-49, p. 71.

Tohmon, R., Shimogaichi, Y., Munekuni, S., Ohki, Y., Hama, Y. & Nagasawa, Y. (1989). Relation between the 1.9 eV luminescence and 4.8 absorption band in high-purity silica glass. *Appl. Phys. Lett.* **54**, 1650–1652.

Turner, T.P., Jones, J.E., Czuchlewski, S.J., Watt, R.G., Thomas, S.J., Metz, D.A., Tallman, C.R., Mack, J.M. & Figueira, J.F. (1990). Configuration and performance of the Los Alamos Aurora KrF/ICF laser system. In *SPIE Proceedings* **1225**, pp. 23–33.

Ueda, K. & Takuma, H. (1988). *Short-Wavelength Lasers and Their Applications*, p. 178. New York: Springer-Verlag.

Von Rosenberg, C.W. Jr. (1992). KrF driver system architecture for a laser fusion power plant. *Fusion Technol.* **21**, 1600–1604.

Webster, D. & London, G.J. (1979). *Beryllium Science and Technology*. New York: Plenum Press.

Williams, R.T. (1989). Optically generated lattice defects in halidecrystals. *Opt. Engg.* **28**, 1024–1033.

Zerby, C.D. & Keller, F.L (1967). Electron transport theory, calculations, and experiments. *Nucl. Sci. Engg.* **27**, 190–218.

Zvorykin, V.D. & Lebo, I.G. (1999). Laser and target experiments on KrF GARPUN laser installation at FIAN. *Laser Part. Beams* **17**, 69–88.

https://doi.org/10.1017/S0263034601194085 Published online by Cambridge University Press